DRFC/CAD

EUR-CEA-FC-1365

FR9001178

TURBULENCE ASSOCIATED WITH SAWTOOTH INTERNAL DISRUPTION

J. ANDREOLETTI, C. LAVIRON, J. OLIVAIN and A.L. PECQUET
F. GERVAIS, D. GRESILLON, P. HENNEQUIN,
A. QUEMENEUR and A. TRUC

May 1989

DRFC/CAD EUR-CEA-FC-1365

TURBULENCE ASSOCIATED WITH SAWTOOTH INTERNAL DISRUPTION

J. ANDREOLETTI, C. LAVIRON, J. OLIVAIN and A.L. PECQUET
F. GERVAIS, D. GRESILLON, P. HENNEQUIN,
A. QUEMENEUR and A. TRUC

May 1989

Article submitted for publication in Nuclear Fusion

TURBULENCE ASSOCIATED WITH THE SAWTOOTH INTERNAL DISRUPTION

J. ANDREOLETTI, C. LAVIRON, J. OLIVAIN and A.L. PECQUET

ASSOCIATION EURATOM-CEA SUR LA FUSION
DRFC CEN-CADARACHE
13108 - SAINT PAUL LEZ DURANCE (FRANCE)

F. GERVAIS, D. GRESILLON, P. HENNEQUIN, A. QUEMENEUR and A. TRUC

PMI ECOLE POLYTECHNIQUE
91128 - PALAISEAU CEDEX (FRANCE)

ABSTRACT

Specific turbulence associated with the sawtooth internal disruption has been observed on TFR tokamak plasmas by analyzing density fluctuations with CO_2 laser light scattering. The time localization is clearly connected with the successive phases of the relaxation process. Some specific turbulence appears in relation to the kink motion, but the main burst corresponds to the collapse phase. We concentrate our study on this strong burst and show first its frequency and wave number spectral properties and the corresponding pseudo dispersion relation. The specific turbulence is spatially localized. It is within the interior of the $q = 1$ surface and extends approximately 120° azimuthally. Taking into account the twisting of the central plasma during the turbulent kink phase, this location agrees with the azimuthal position of the "sooner and faster" outgoing heat flux. The power level of this turbulence is two orders of magnitude larger than the local quasi-stationary turbulence. These observations are in fair agreement with the predictions of the sawtooth disruption model previously proposed by Andreoletti. The observed specific turbulence shows several similarities with the so called "magnetodrift turbulence" described in the model.

1. INTRODUCTION

Since its first experimental observation by Von Goeler et al. [1], sawtooth phenomenon, also referred to as internal disruption, has remained an active research area. From the experimental point of view, observation of sawteeth can give useful information on the location of the $q = 1$ surface, and provides a direct measure of the thermal diffusivity coefficient through the resulting heat pulse propagation. However, the central confinement is periodically degraded by the sawtooth, limiting the maximum achievable central temperature and density. The sawtooth amplitude usually increases when additionnal heating is applied, leading to a limitation of the performance in the reactor issue. Although a lot of theoritical work has been devoted to the subject over the last fifteen years [2 to 17] we have to conclude that none of the theoritical models put forward so far are in agreement with all the experimental data [18]. Moreover, understanding of the sawtooth phenomena was further confused by some recent observations such as precursorless sawteeth, crescent deformation of the core, central q values varying weakly and being much less than unity, partial sawteeth, snake behavior, etc ...

Historically the first tentative interpretation proposed in 1974 by Von Goeler suggested that the $m/n = 1/1$ internal kink mode could be responsible for the relaxation [1]. But the existing stability calculation [2] was limited to a cylindrical geometry in which the internal kink is mainly a current driven mode, unstable even for a zero pressure. Furthermore the non linear evolution of this mhd motion appeared to be limited by flux conservation to a very small amplitude [3]. To remedy this amplitude limitation, Kadomtsev proposed [4] that an island forms by resistive tearing mode and reaches the magnetic axis. This reconnection at an hyperbolic axis of the helical flux inside the $q = 1$ surface to that outside is supposed to be accelerated by the formation of a narrow current layer. Numerical simulations of the Kadomsev model confirmed its potential [6, 9]. We note that such a "full reconnection" model implies that if $q < 1$ before the relaxation, we must have $q > 1$ after. Simultaneously several articles were devoted to the stability of modes, the possible triggers of the sawtooth. They concern the ideal toroidal 1/1 kink mode [5] and the resistive kink mode [8, 9, 14]. Interpreting sawteeth measurements, TFR Group expressed some doubts about the validity of the Kadomsev model. In a

proposal by Samain [7] and Dubois, Samain [11], the final collapse was attributed to the onset of fine scale resistive mhd turbulence initiated by a current sheet appearing all along the two branches of the island separatrix, and propagating radially inwards and outwards. In a more recent proposal by Wesson [13], the shear is supposed to be so small ($1-q \sim 10^{-2}$) that the mhd kink can fully develop without any reconnection.

Recent observations by a tomographic treatment of two orthogonal soft X-ray cameras lead to a two dimensional image of the dynamical process taking place during the relaxation [19 to 21]. They clearly show the large scale smooth convective cells of the kink like motion. In addition to these phenomena, we have recently reported the observation of a specific turbulence associated with the sawtooth crash [22 to 25]. In these reports, the time synchronism and frequency spectrum of this turbulence were given. In the present article a more detailed study is reported. We show that the turbulence is radially and azimuthally localized. The extension of the turbulent cell and its relative localization with respect to the kink motion are given. The level of the observed turbulence is estimated relative to the quasi-stationary one. A comparison with a theoretical model [26-27] is discussed.

The paper is organized in the following way. We start by a rapid description of the experiment (Ch. 2). Ch. 3 recalls the main characteristics of the quasi-stationary turbulence in order to be able to isolate the sawtooth specific turbulence contribution from the global signal (Ch. 4). The central part of the paper (Ch. 5) concerns the experimental description of the turbulence during the collapse. Ch. 6 considers the heat flux asymmetry observed during the crash and its relation with the specific turbulence. In Ch. 7, we discuss the main results in the frame of the magnetodrift sawtooth model proposed by Andreoletti. Some concluding remarks end the paper.

2. EXPERIMENTAL PROCEDURE

The reported experiments have been performed on the TFR tokamak, a medium size machine (R = 1 m ; a = 0.2 m) with a circular cross section. They concern standard ohmically heated discharges e.g. 4.5 T, 240 kA, average density 6.10^{19} m^{-3}, central electron temperature of 1.4 keV and central ion deuterium temperature of about 0.8 keV. The Zeff values are typically around 2. The discharge lasts about 0.5 second and the electron energy confinement time is about 25 ms.

Sawtooth behaviour is observed throughout the discharge for most operating conditions after the current profile has peaked. The main diagnostic used to study sawteeth is an array of 26 soft x-ray (SX) detectors, viewing the plasma from above. The array has a spatial resolution of about 1.5 cm at the midplane and views the plasma from 15 cm inside the equilibrium major radius to 16 cm outside. A description of this SX system can be found on Ref. [28].

Detection of the density fluctuations is made with a conventional coherent scattering apparatus usually employed to measure the quasi-stationary low frequency turbulence [29]. A 3W CO_2 single mode laser (λ_i = 10.6 μm), with a beam radius w_o = 1.3 cm in the plasma is used. The beam crosses the plasma vertically and can be scanned across the major radial direction from X = -4 cm to X = +8 cm, with the negative values corresponding to the high field side of the plasma. The collected signal is emitted from a vertical chord of the plasma. The scattering angles are variable between 0.5 and 3 mrad, thus allowing measurements of horizontal wave numbers k between 3 and 20 cm^{-1}. The detector current i(t) is proportional to the instantaneous space Fourier transform, with a k density fluctuation wave vector. It is fed to a fast digitizer (100 MHz ; nx32 Kwords buffer) and sent to the TFR main computer. After signal processing, we get the scattered power quantitatively proportional to the Fourier transform $S_k(\omega)$ of the space and time autocorrelation function of the fluctuating density $\tilde{n}(r,t)$.

The scattering set up and soft X-ray port are separated toroidally by 90° and the sign of the poloidal rotation is positive or negative, depending on the relative positions of the two diagnostics and the directions of the current and main magnetic field.

3. "QUASI STATIONARY" TURBULENCE

Because there is a partial overlapping between the new specific turbulence and the quasi-stationary (QS) one, we have to recall in some detail the main properties of the usual QS turbulence : ω and k spectra, "intermittency", radial profile. The power spectrum of usual density fluctuations emitted from a plasma diameter is well approximated by four linear sections [29], separated by three frequencies f_1, f_2, f_3, in a double log scale representation : $\log S_k = F(\log f)$ as shown in fig. [1]. Although the spatial localization cannot be measured along the direction of the laser beam (vertical direction), we can make a conjecture that the spectrum is made of different portions, each associated with one particular zone. The partial spectra of these emissive zones are schematically shown on fig. 1 as dashed lines. The low frequencies ($f \lesssim f_1$) are associated with the outer zone, the intermediate frequencies ($f_2 \lesssim f < f_3$) with the gradient zone while the high frequency tail ($f > f_3$) is attributed to the central region. Several subsidary observations sustain such a conjecture :

i) During some ICRF auxiliary heating experiments, a large increase of the low frequency part of the spectrum was observed every time a strong interaction of the plasma with the limiter was noticed [30], suggesting a link between the low frequency behaviour and the outer region of the plasma.

ii) When the scattering volume of observation is moved to a vertical chord away from the centre of the plasma ($r/a \sim 2/3$) the high frequency part of the spectrum ($f > f_3$) disappears.

iii) During pellet injection experiments ablated in the gradient zone, the fluctuations increase mainly in the intermediate frequency zone.

iiii) Using phase contrasts as an imaging technique for plasma density fluctuations, Weisen [31] clearly shows that the low frequency part of the spectrum preferentially stems from the outer plasma zones.

Associated k spectrum variations, after frequency integration, have been previously published [29]. These exhibit an amplitude maximum for $k = 5\ cm^{-1}$, and two apparent decaying slopes for higher k values (fig. 2). The decaying $k^{-2.2}$ slope is considered to be significant, however the apparent second observed slope $k^{-4.5}$ is mainly due to a reduction of the scattering volume. Indeed if the fluctuation wavevectors are perpendicular to the B field line, only those parts of the scattering volume where the observed $k \pm \Delta k$ is perpendicular to B can contribute to a signal. For $k \geq 20\ cm^{-1}$ the relative wave number resolution $\Delta k/k \leq 0.07$ becomes smaller than the magnetic line angle $\alpha = \frac{B_p}{B_t}$. Then the effective scattering volume is reduced and does not coincide anymore with a full vertical chord. This effect tends to increase the k exponent. The true value is somewhat smaller.

Quasi-stationary behaviour is only an average property. If we examine the time sequence in more details by fragmenting the frequency spectrum, we observe "intermittency" [32]. This is not very pronounced near the intermediate frequency f_2 but it is more important in the low frequency part of the spectrum (near f_1). In typical TFR plasmas, the successive bursts last for Δt equal 30 to 60 μs at intervals of t separated by 150 to 250 μs (fig. 3).

Moreover, the fluctuation amplitude is strongly nonuniform. Many experiments have shown that the relative density fluctuations are an increasing function of the radius with central values in the range $\tilde{n}/n \sim 1$ to 3.10^{-3} and edge values $\tilde{n}/n \geq 10^{-1}$ (see for exemple [33]).

4. SPECIFIC DENSITY FLUCTUATIONS

4.1 Time analysis : the four phases

During internal disruptions, specific density fluctuations have been detected [22]. They consist principally of a high frequency spectrum (0.5 MHz $\leq f \leq 2.2$ MHz for $k = 7$ cm^{-1}) which is superimposed on the quasi-stationary turbulence previously reported. However, a more comprehensive study shows an evolution of the specific turbulence during the various phases of the internal disruption as observed from the soft X-ray radiation signals.

Four phases in the disruption process can be identified. The first shows a precursor oscillation and can possibly be strongly shortened. The second corresponds to a helical displacement of the hot core. The third shows a fast drop of the central emissivity with a poloidal expansion of the hot core and, in the fourth one, the plasma tends to recover its poloidal symmetry. The evolution of the turbulent signal mean square amplitude, for $k = 5$ cm^{-1}, filtered between 0.4 to 3.1 MHz, is shown on fig. 4. The traces (a) to (e) refer to the soft X-ray signals stemming from various chords while (f) refers to the power of the filtered scattering signal.

- An $m = 1$ precursor oscillation is seen. No correlated particular modification appears on the density fluctuations.

- The fast displacement of the hot core is observed as a decay of the X-ray signal (b) and an increase of signal (d). During this phase, a noticeable increase of the turbulent signal is detected. The duration of this period ranges typically from 15 to 20 microseconds.

- The third phase, lasting 20 microseconds, corresponds to a rapid drop of the central emissivity and to a heat pulse expelled outside the inversion radius (traces (a) and (e)). We notice an asymmetry in the process : the energy flow appears sooner and faster on chord (a) than on chord (e). During this phase, the power level of the turbulence increases considerably. It is maximum in the middle of this period and then decreases to a value close to the one at the end of the second phase.

- The last phase is associated with a profile reorganisation. The heat flow continues on chord (e). During this last phase, covering about 20 microseconds, the amplitude of the turbulence is comparable to the one during the preceeding phase.

4.2 Frequency spectrum in the four phases

The spectral composition of the fluctuations is not the same during the successive phases.

The weak specific turbulence, clearly observed in relation to the turbulent kink phase (phase 2) corresponds to frequencies $f \sim f_2$ previously described ; i.e. 400 kHz $\leq f \leq$ 600 kHz for $k = 5\ cm^{-1}$. Below 400 kHz the observation is masked by the part of the QS spectrum attributed to the gradient zone turbulence. Nevertheless, a few examples show that an increase of the fluctuations during the same period of time can be seen down to 200 or 250 kHz. These observations suggest a frequency domain approximately two times lower than the one of the main burst during the collapse (see next section).

Estimation of its power level may also be difficult. For the part above 400 kHz, we notice : $\langle \tilde{n}^2 \rangle_{kink} \sim 1/30\ \langle n^2 \rangle_{collapse}$. Amplitude and frequency spectrum of the fluctuations observed during the last phase (the return) are similar.

The strong burst associated with the collapse (phase 3) is due to frequencies greater than f_2. It will be the object of a detailed analysis presented in the next chapter.

5. TURBULENCE DURING THE COLLAPSE

5.1 Spectral properties

The properties of these fluctuations will be described according two complementary approches. Spectral analysis is used for the smaller scale properties (which are not directly accessible in space -

time, and are more irregular) whereas spatio-temporal analysis will be used for the domain where the process is localized.

a) Frequency spectrum

A 20 microsecond period for the scattered signal is necessary to compute a Fourier analysis and define a "quasi instantaneous" spectrum of turbulence. Excluding the time duration of the internal disruption, thirty successive "quasi instantaneous" spectra preceding the crash and thirty others following it are performed, and averaged to define a mean spectrum $(S_k)_{av}$ of the quasi-stationary turbulence (fig. 5a). It is important to note that the shape and the amplitude of the spectrum prior and after the disruption are identical, showing that the specific turbulence and QS turbulence are two uncorrelated processes. A spectrum $S_k(\omega)$ is performed during the collapse phase (drop of the central temperature) (fig. 5b). The difference $\Delta S_k(\omega) = S_k(\omega) - (S_k(w))_{av}$ is attributed to the associated sawtooth turbulence (fig. 5c). It essentially contains high frequency components. In the particular example shown in (fig. 5c), $\Delta S_k(\omega)$ covers the frequency range 390 kHz $\leq f \leq$ 1200 kHz and presents a maximum around 610 kHz. The amplitude for frequencies below f_c = 390 kHz retain an average value equal to zero. They exhibit the usual variations of the "quasi instantaneous" spectrum which are not significant.

For a fixed wave number, the shape of this ΔS_k spectrum is quite constant and does not depend on the considered disruption. After an integration over frequency, we can compute the mean quadratic value $\langle \Delta\tilde{n}^2 \rangle$ of the specific density fluctuations associated with the collapse. In this example, $\langle \Delta\tilde{n}^2 \rangle$ largely exceeds $\langle \tilde{n}^2 \rangle_{av}$ ($\langle \Delta\tilde{n}^2 \rangle / \langle \tilde{n}^2 \rangle_{av} \sim 1.7$), demonstrating the importance of this new turbulence.

b) Wave number spectrum

In contrast to the shape of the frequency spectrum, the density fluctuation level $\langle \Delta\tilde{n}^2 \rangle$ varies widely from one disruption to another, values scattered from 1 to 10 for comparable disruptions. In spite of this large dispersion, we observe an average decay of $\langle \Delta\tilde{n}^2 \rangle$ for increasing values of k in the analysed domain ($5 \leq k \leq 17$ cm^{-1}) (fig. 6). In the double log scale, the mean trace is a line of slope = -5 ± 1, showing a $k^{-5 \pm 1}$

variation law. This result is confirmed by several simultaneous measurements of two wave numbers (5 and 17 cm^{-1}).

c) Dispersion relation

For a given wave number, the frequency spectrum is widely spread. However, we can trace a "pseudo" dispersion relation corresponding to the maximum of the frequency spectrum as a function of k Fig. 7 shows such a dispersion curve. The dots mainly correspond to the analysis of several disruptions although some of them correspond to the analysis of two simultaneously measured k numbers in the same disruption (k = 5 and 17 cm^{-1} for example). It is possible to define a mean phase velocity $V_s \sim 8.10^3$ m/s which is significantly greater than the phase velocity of the quasi-stationary fluctuations $V_{QS} \sim 2.3\ 10^3$ m/s shown on the same diagram. As already discussed [29] and deduced from fig. 1, the phase velocity of QS turbulence in the central region is inferred to be even smaller ($\sim 1.5\ 10^3$ m/s).

5.2 Spatial localization

For a fixed wave number we have analysed many disruptions corresponding to several positions X of the observation chord and plot $\langle \Delta\tilde{n}^2 \rangle$ as a function of X (fig. 8). The envelope of the various points gives a first estimation of the radial localization of the turbulence. No signal is detected outside the q = 1 surface and a depression of the amplitude is apparent around X = 0, suggesting that the turbulence is located somewhere inside the q = 1 surface. A rough estimation of the width of the turbulence domain can be deduced from the experiment and tends to be on the 2 cm scale. The large dispersion of the points on fig. 8 for a given value of X suggests an azimuthal localization of the turbulence.

a) Azimuthal localization

We shall separate the r and θ variables, which come to assume that the emitting cell has a bean shape, centered on a surface of radius r_0 with a characteristic radial extension Δr and a poloidal extension $\Delta\theta_c$ (see fig. 9). From the raw experimental points on fig. 8 we choose r_0 = 3 cm. By following the m = 1 mode observed on the soft X-ray signals just at the

interior of the inversion radius, say trace b of fig. 4 ($r \leqslant r_1$), the azimuthal position of the cold side at the beginning of the second phase (fast displacement of the hot core) is called θ. For one particular X position of the scattering volume and one k wave number, we analyze $\langle \Delta\tilde{n}^2 \rangle$ as a function of $(\theta - \theta_0)$, θ_0 being the azimuthal angle of the r_0 circle intersection with the axis of the scattering volume. The data are symmetrical. Under these conditions, we choose $(\theta - \theta_0)^2$ as a new variable. Fig. 10 and 11 show such a study for two X positions. Data stemming from positive and negative values of $(\theta - \theta_0)$ are represented by different symbols. The amplitude depends drasticaly on $(\theta - \theta_0)^2$. It is maximum for $\theta = \theta_0$, with an experimentally observed half width of $\Delta\theta \sim 60 \pm 10°$ for $k = 5\ cm^{-1}$ (fig. 10) and $70 \pm 10°$ for $k = 7\ cm^{-1}$ (fig. 11). From this analysis, we conclude that the turbulence is azimuthally localized on the cold side.

b) Radial localization

The maximum amplitude of the turbulence is observed when $\theta = \theta_0$, i.e. when the axis of the scattering volume coincides with the centre of the turbulence cell. When no such experimental points exist, extrapolation of the line on fig. 10 is used to estimate the maximum amplitude. These estimated maxima are reported as crosses on fig. 8. They fall on an envelope (the dashed line). From this azimuthal and radial analysis, we conclude that the fluctuations exist in a cell localized around a ring of radius $r_0 \sim 2.5\ cm \sim 0.5 r_{q=1}$.

c) High field side - Low field side symmetry

A careful analysis of the azimuthal law of variation of $\langle \Delta\tilde{n}^2 \rangle$ for two symmetrical X positions with respect to the magnetic axis have been performed (Fig. 11). Although the points gained from the outside chord quasi systematically exceed the inner ones, both signals are close and do not allow conclusions about the existence or not of a ballooning in the amplitude. The radius of the cell localization, compared to the diameter of the scattering beam, is too small in TFR. This study should be undertaken on a bigger machine.

d) Numerical deconvolution

The collected signal stemming from the various scattering volume elements is the result of a convolution in the Fourier space of the turbulence cell characteristics and of the probing laser beam. The object of this section is to estimate the intrinsic properties of the turbulence (spatial localization and k spectral properties).

For a given wave number k, the measured quadratic mean value of the fluctuating density associated to the sawtooth is :

$$\langle \Delta\tilde{n}^2 \rangle = \alpha \left| \int \Delta\tilde{n}(\bar{r})\ U(\bar{r}) \exp -(i\bar{k}.\bar{r}) \quad dr \right|^2 = \alpha \left| \int \Delta\tilde{n}(\bar{k}')\ U(\bar{k}-\bar{k})\ dk' \right|^2$$

where $\Delta n(r)$ is the local specific fluctuating density and $U(r)$ is the normalized local laser beam profile given by two projected gaussian functions in a plane perpendicular to its direction of propagation i.e.

$$U(\bar{r}) = U_0 \exp - ((x-X_0)/W_0)^2 \exp -(z/W_0)^2$$

The analysis is limited to the poloidal plane (in the toroidal direction, the turbulence is assumed to have a characteristic length large compared to the beam diameter and will appear as a constant).

If we assume that, on the scale of the beam size, the turbulence has a locally isotropic spectrum in k_x, k_z Fourier space, the computation is reduced to a convolution between the spatial amplitude distribution of the turbulence and the beam profile. We take for the turbulence amplitude two gaussian functions, in the radial r and azimuthal θ directions, respectively centered around r_0 and θ_c i.e.

$A_{turb.} = A_0 \exp -((r-r_0)/\Delta r)^2 \exp -((\theta-\theta_0)/\Delta\theta_c)^2$ and determine numerically the values of r_0, Δr and $\Delta\theta_c$ which give a good agreement with the experimental results.

A better agreement is obtained if we assume a radially asymmetric gaussian function for the turbulence, with a characteristic width smaller for small radii. As is shown on fig. 12a good fit is found for :

$r_0 = 1.7$ cm ; $\Delta\theta_c = 1.2$ rad
$\Delta r_i = 0.3$ cm for $r < r_0$; $\Delta r_e = 2$ cm for $r > r_0$

Several k spectra have been tested. The result from this analysis is that an isotropic spectrum is probably present. We note that a purely radial turbulence is inconsistent with the observtions and can be definitively discarded. Conversely, a purely azimuthal turbulence can account for the experiments with $r_0 \sim 3$ cm and $\Delta r_i = \Delta r_e = 2$ cm.

Consequently, we conclude that an approximately isotropic spectrum is present, on which a partially azimuthal contribution could be superimposed. Only part of the k spectrum of this turbulence has been measured. The k spectrum covers at least the $k = 5$ cm^{-1} to $k = 17$ cm^{-1} domain ($k\rho_i \sim 0.5$ to 1.5) and is a rapidly decaying function of k.

5.3 Power level

The amplitude of the specific fluctuations will not be evaluated in absolute terms, but rather compared with the local quasi-stationary fluctuations present in the central region. The essential element in this discussion is the fact that the measured fluctuations come from volume elements positionned along a chord (here a diameter) through the plasma. In order to make our estimation, the radial domain is divided in three regions : a central region (symbol C) for $r/a < 0.4$, a gradient region (symbol G) for $0.4 < r/a < 0.9$ and an edge region (symbol E) for $0.9 < r/a < 1.1$.

In these conditions, and assuming that the fluctuations from different regions are not correlated, the total Q.S. collected fluctuations are in quadratic mean value :

$$\langle\tilde{n}^2\rangle = \langle(\int_E dl\ \tilde{n})^2\rangle + \langle(\int_G dl\ \tilde{n})^2\rangle + \langle(\int_C dl\ \tilde{n})^2\rangle \text{ or}$$

$\langle\tilde{n}^2\rangle = \langle\tilde{n}^2\rangle_E + \langle\tilde{n}^2\rangle_G + \langle\tilde{n}^2\rangle_C$ if the short notation $\langle\tilde{n}^2\rangle$ is used in place of $\langle(\int dl\ \tilde{n})^2\rangle$.

Admitting that the radial variation of the relative density fluctuations in a Tokamak is well represented by the information gathered by Liewer on fig. 8 in her review article [33], we have the approximate relation : $\left(\frac{\tilde{n}}{n}\right)_E / \left(\frac{\tilde{n}}{n}\right)_C \sim 30$ to 50. Taking into account the observed density profile such that $n_C/n_F \sim 6$ and the relative length of the concerned regions, we get $\langle\tilde{n}^2\rangle_E \sim 10\ \langle\tilde{n}^2\rangle_C$. A similar estimation for the gradient and edge regions gives : $\langle\tilde{n}^2\rangle_G \sim \langle\tilde{n}^2\rangle_E$. Thus for the total Q.S. fluctuations we have $\langle n^2\rangle \sim 20\ \langle\tilde{n}^2\rangle_C$.

For the example shown on fig. 5 the ratio between the radially integrated specific $\langle\Delta\tilde{n}^2\rangle$ and the total Q.S. density fluctuations is such that $\langle\Delta\tilde{n}^2\rangle/\langle\tilde{n}^2\rangle \sim 1.9$. For a well centered cell ($\theta = \theta_0$) the graph of fig. 10 gives by extrapolation $\langle\Delta\tilde{n}^2\rangle/\langle\tilde{n}^2\rangle \sim 2.5$ and so $\langle\Delta\tilde{n}^2\rangle/\langle\tilde{n}^2\rangle_C \sim 50$.

This ratio applies to fluctuating densities integrated on appropriated volumes of scattering. For the specific fluctuating density it is the cell volume included in the diagnosing beam. Taking into account the dimensions and the position of the cell we find that this volume is approximately one half of the scattering volume for the Q.S. fluctuations in the central region. Then the evaluation of the ratio between the local values of the specific and Q.S. fluctuations gives :

$$\langle\Delta\tilde{n}^2\rangle/\tilde{n}^2_C \sim 100 \text{ to } 200.$$

The fact that the specific fluctuations appear to be maximum for $k < 5\ cm^{-1}$ whereas QS turbulence is maximum for $k \sim 5\ cm^{-1}$ could increase this ratio a little.

Assuming a central QS relative density fluctuation equal to 1 to 3.10^{-3}, the specific fluctuation is estimated to reach the value $(\Delta\tilde{n}/n)_c \sim 2$ to 3.10^{-2}.

We conclude that the specific fluctuations, whose power is two orders of magnitude greater than the local QS turbulence, represent a strong phenomenon. Therefore the corresponding turbulence appears a good candidate to explain the strong increase of the transport during the collapse. Indeed, we estimate the heat coefficient during the collapse as $\chi_{collapse} \sim r^2_{q=1}/4\ \tau_{collapse}$ where $r_{q=1} = 5$ cm and $\tau_{collapse} \sim 20\ \mu s$, then :

$$\chi_{collapse} \sim 3.10^5\ cm^2/s \sim 100.\chi_{q.s.}$$

6. HEAT FLUX ASYMMETRY

During the collapse, the heat flux outside the $q = 1$ surface is not azimuthally symmetrical. This asymmetry can be seen on the SX signals. We recall that a displacement parallel to the line of sight of the X-rays beams cannot be observed, whereas a motion perpendicular to the observation line is fully detected. For example on fig. 4 the heat flux appears "sooner and faster" on chord (a) compared to chord (e). On the rose of fig. 13 we note for each observed sawtooth the direction of the "sooner and faster" heat flux by an arrow with an amplitude proportional to the sharpness of the asymmetry. Assuming an unmodified rotation velocity of the hot core during the kink, the heat flux appears to be directed $3\Pi/4$ away of the hot side, i.e. apparently at one corner of the turbulence cell.

This result appears somewhat surprising at first glance. However, if we apply Andréoletti's model [see next chapter], the plasma rotation could be modified by the turbulent kink. The rotation of the edge part ($r \lesssim r_1$) slows down whereas the one of the most central part speeds up, producing a twisted state. A subsidary observation tends to confirm the existence and the large value of the twisting. We again draw, from the SX signals, a rose indicating the apparent direction of the fast kink displacement with respect to the azimuthal position of the precursor asymmetry (fig. 14). The result is the fast kink is seen as if it was directed at $\Pi/2$ in advance with respect to the precursor. This can be

explained by a composition of the kink displacement and an accelerated rotation of the hot core (~50 to 60°). The estimated twisting angle is large on TFR (~ Π/4) because the plasma rotation is fast. Under these conditions, the azimuthal direction of the "sooner and faster" heat flux would coincide with the central position of the turbulent cell (fig. 15). On large machines the plasma rotation is much slower and thus twisting is much less pronounced but visible [19 to 21].

The coincidence between the direction of the "sooner and faster" outwards heat flux, and the centre of the turbulence cell is a strong experimental element in favour of the increased diffusivity being due to this turbulence. Measurements performed on a large machine having a slowly rotating plasma would give a more direct access to this information without being confused by an additional rotation.

7. COMPARISON WITH MAGNETODRIFT TURBULENCE

A qualitative turbulent model has been proposed by Andreoletti as a tentative explanation of the sawtooth mechanism [26, 27]. Here, we do not recall the arguments exposed by the author to justify the model, but propose only to discuss the main elements correlated to the above mentioned experimental data.

Magnetodrift (md) turbulence is the essential ingredient of the model. It implies a two fluids dynamical representation and can exist only in configurations having a sufficient large scale asymmetry of the local magnetic shear. The wave number spectrum perpendicular to $\bar{B}$ is quasi-isotropic, and the mean wave number parallel to $\bar{B}$ is related to the local value s_* of the shear parameter : $k_{\parallel} \sim 2\Pi\, s_* /qR$. Along $\bar{B}$ lines, md motions agree with mhd dynamics where the local magnetic shear is weak, and with drift wave dynamics where the local shear is strong.

Four phases are defined : resistive kink, turbulent kink, collapse, return. We shall now compare the predictions of the model successively for each of the four phases, using our observations of soft X-ray and specific density fluctuations.

a) The resistive kink

Just after the preceeding relaxation the pressure gradient inside $r = r_{q=1}$ is small, and according to the model the shear parameter $\hat{s}_1$ at $r = r_{q=1}$ is also small. During the regeneration period they increase and the threshold for the resistive kink instability can be reached. The growth rate for the resistive kink, taking into account diamagnetic and rotation effects [9] gives $\gamma \sim 4.10^3\ s^{-1}$. This is a little faster than the observed evolution of the precursor oscillation whose growth time is $\tau \sim 300$ to 400 μs.

b) The turbulent kink

According to the model, the asymmetry of the local magnetic shear produced in the resistive sheet, and the high velocity shear of the return flux give rise to inertially driven md turbulence. This turbulence triggers a fast transition from resistive kink to quasi-mhd kink and allows its catastrophic increase. The interplay between the large scale kink instability that drives md turbulence and this md turbulence that produces magnetic relaxation permits the full development of the convective motion.

The radial velocity of the fast kink observed during the TFR sawteeth is approximately $V_r \sim 2.10^5$ cm/s. The velocity of the return velocity flux for smooth convective cells as observed on JET tomography pictures is estimated to be $V_\theta \sim 2V_r \sim 4.10^5$ cm/s [21]. The typical frequency of the inertially driven turbulence will be such that $\omega \sim kV_\theta$. For $k = 5\ cm^{-1}$ this gives $f = 300$ kHz, a value that could agree with our experimental estimations given in section 4.

The velocity fluctuations are expected to be (in similarity with hydrodynamics) about half an order of magnitude smaller than the return stream velocity.

$\delta V \sim 1/3\ V_\theta \sim 4/3.10^5$ cm/s. From the relation $\delta V \sim k\delta\Psi/B \sim k\rho_i V_i\ T_e/T_i\ e\ \delta\Psi/T_e$ we get for the density fluctuations the rough estimate $\frac{\tilde{n}}{n} \sim \frac{T_i}{T_e}\ \frac{1}{k\rho_i}\frac{\delta V}{V_i} \sim 6.10^{-3} \sim 3\ (\tilde{n}/n)_{QS}$ and so $\langle\tilde{n}^2\rangle_{kink} \sim 10\ \langle\tilde{n}^2\rangle_{QS}$. Our experimental estimate for the non hidden part (400 kHz < f < 500 kHz) is :

$\langle\tilde{n}^2\rangle_{kink} \sim 1/30\ \langle\tilde{n}^2\rangle_{collapse}$ $1/30.(100\ \text{to}\ 200).\langle\tilde{n}^2\rangle_{QS} \sim 5\ \langle\tilde{n}^2\rangle_{QS}$. So an agreement between both estimations of $\langle n^2\rangle_{kink}$ is possible if we suppose that fluctuation power in the generally masked part (200 kHz < f < 400 kHz) is of the same order as the one of the visible part.

The plasma rotation will be modified by the turbulent kink. We shall first remark that the observed plasma potential is generally negative [34], showing that in the usual quasi-stationary regime the electron gas confinement is better that the ionic one. In the md turbulence domain, magnetic surfaces no longer exist because of the non mhd part of δB. The electrons can escape along $\vec{B}$ lines and the local electric charge density will become positive. The resulting modification of the plasma potential profile tends to produce a slowing down of rotation in the region $r < r_{q=1}$ and an enhancement of rotation of the central core, giving rise to some twisting of the plasma.

c) The collapse

The collapse of the temperature and density profiles is due, in the model, to a strong burst of md turbulence. The occurence of this burst is related to some threshold in the helical asymmetry of the local magnetic shear. This turbulence is mainly located in the wake of the kink motion, and could explain the cold bubble formation and the crescent distortion of the hot core [19].

As we have seen in the discussion of section 6, the azimuthal positions of respectively the observed turbulent cell and the "sooner and faster" heat flux are not precisely opposite to the hot spot position during the collapse. They present a phase lag of approximately $\Pi/4$ relative to the direction of plasma rotation, and the model suggests an explanation of this angular discrepancy by the twisting effect.

The numerical deconvolution indicates a radially asymmetrical turbulence cell for the case of an isotropical wave number spectrum. Part of this rather strong asymmetry could result from the tips of the bean shape related to our method of separation of the two variables r and θ.

The md turbulent motions are supposed to be well represented by mhd dynamics in the wake, and by drift wave dynamics on the side and in front of the kink displacement. The local magnetic shear parameter s_* on the side being approximately equal to the initial global shear $\hat{s}$. We have for the frequency the estimate :

$$\omega = k_{\parallel} \sqrt{\overline{V_i V_e}} \sim 2\Pi \frac{\hat{s}}{qR} \sqrt{\overline{V_i V_e}}$$

In the proposed model, the magnetic shear s increases during the turbulent kink and we assume that, at the end of this phase, its value has become similar to the one of a regular current density profile. This gives us $\hat{s} \sim 0.25$ for $r < r_{q=1} \sim a/3$. This gives : $f \sim 0.25/100$ cm $(3.10^7$ cm/s . 2.10^9 cm/s$)^{1/2} \sim 0.6$ Mhz, in good agreement with our observations.

The level of the specific fluctuations during the collapse as observed experimentally has been estimated (section 5) to reach the value $\Delta n/n \sim 2$ to 3.10^{-2}. This is more than the usual estimate from comparison of the perturbed and initial gradients $\Delta\tilde{n}/n \sim 1/k_r n \sim 10^{-2}$ and it is one third to one half of the initial density bump $\Delta n/n \sim (r_{q=1}/a)^2 \sim 6.10^{-2}$. The numbers suggest that the observed strong fluctuations are in an extreme non linear regime in which the quadratic term $\delta V.\nabla\delta n$ is of the same order as the linear ones. This corresponds to $\delta V \sim \omega/k$ and gives the estimate $(\tilde{n}/n)_{NL} \sim \frac{T_i}{T_e} \quad \frac{1}{k\rho_i} \frac{\omega/k}{V_i} \sim 3.10^{-2}$.

We have seen (section 5.1b) that between $k = 5$ cm^{-1} and $k = 17$ cm^{-1} specific turbulence is strongly decreasing $\sim k^{-5}$. We can then guess that the maximum of the wave number spectrum coresponds to a k value less than 5 cm^{-1}, say 4 or 3 cm^{-1}. As to the large scale kink, the known crescent deformation includes harmonics at least $m = 2$, $m = 3$ which correspond to $k > 1$ cm^{-1}. We observe that the unknown interval appears rather small. This remark, and the fact that the estimated density fluctuation is a large fraction (1/3 to 1/2) of the initial density bump, suggest that there may be no gap between the large scale and small scale motions, but we have no direct proof of that.

d) The return

When the pressure gradient has vanished md turbulence dies away. According to the model, the return of the magnetic structure to a quasi-circular axisymmetrical shape must be fast and will produce a new burst of md turbulence similar to the one during the turbulent kink phase, resulting in the formation of an annular plateau $q \sim 1$. Our observations have shown that in fact specific turbulence density fluctuations are similar during the kink and return phases.

8. CONCLUSION

In the sawtooth internal disruption process, four phases can be identified. The last three are characterized by the occurence of an extra turbulence which superimposes on the quasi-stationary one. During the collapse phase, this extra turbulence is very strong, localized inside the $q = 1$ surface. The turbulence cell has a radial extension of a few cm and an azimuthal extension of one third of a turn. It is located at the cold area and coincides with the azimuthal location of the sooner and faster heat flux.

This specific turbulence appears as a transition between drift type and mhd turbulence. Its frequency components and phase velocity are about four times higher than the quasi-stationary ones. Its amplitude is two orders of magnitude larger than the local QS one and could easily explain the high value of the heat diffusivity factor observed during the collapse.

It is clear that all these observations agree with the model proposed by Andreoletti. However, the credibility of the main theoretical concepts of the model still needs more formalized and more quantitative treatments.

Acknowledgements

The authors would like to thank TFR group's members for their active participation in the TFR experiments reported here. Thanks to J. How for his proof reading.

FIGURE CAPTIONS

Fig. 1 Average density fluctuation spectrum of the quasi-stationary turbulence versus frequency for a central chord ($k = 5\ cm^{-1}$, frequency bandwith $\Delta f = 6$ kHz).

The dotted lines correspond to conjectured spectrum associated with the different plasma zones $\langle \tilde{n}^2 \rangle_{av} = \int (S_k)_{av}\ df$ = mean quadratic value of the quasi-stationary density fluctuations.

Fig. 2 Wave number spectrum of the quasi-stationary turbulence for a central chord.

Fig. 3 Time evolution of a filtered frequency band of the quasi-stationary turbulence : "intermittency".

Central frequency = 100 kHz, $\Delta f = \pm 30$ kHz ; $k = 7\ cm^{-1}$.

Fig. 4 Temporal evolution of soft X-ray signals and of specific density fluctuations during the different phases of the sawtooth crash.

- a to e are soft X-ray signals for different chords from inner to outer side of the torus. r_1 is the inversion surface radius. The portions of the soft X-ray signals characteristic of the three last phases are in bold type.
- f shows the density fluctuations filtered between 0.4 to 3.1 MHz for a central chord ($k = 5\ cm^{-1}$).

Fig. 5 Determination of the specific turbulence spectrum (central chord ; $k = 5\ cm^{-1}$).

a) Average frequency spectrum $(S_k)_{av}$ of the quasi-stationary turbulence ($\Delta f = 24$ kHz ; $\langle \tilde{n}^2 \rangle_{av} \propto \int (S_k)_{av}\ df$).

b) Frequency spectrum S_k of the total turbulence during sawtooth crash ($\Delta f = 24$ kHz).

c) Frequency spectrum of the specific turbulence :

$\Delta S_k = S_k - (S_k)_{av}$; the significant spectrum is for frequencies greater than f_c.

Fig. 6 Wave number spectrum of the specific turbulence (central chord).

Fig. 7 Dispersion curves of the turbulence (central chord).

a) Quasi-stationary turbulence ; mean phase velocity $v_{QS} \sim 2.3\ 10^3$ m/s.

b) - Specific turbulence ; mean phase velocity $V_{st} \sim 8 \pm 2\ 10^3$ m/s.

Fig. 8 Radial scanning of the specific turbulence for $k = 7\ cm^{-1}$. The different points corresponding to a same position are obtained from various identical crashes.

Crosses are deduced from fig. 10 and refer to azimuthal angle $\theta = \theta_0$. The dashed line represents the estimated radial variation of the specific turbulence for $\theta = \theta_0$.

Fig. 9 Main parameters. Schematic view of the turbulent cell and of the scattering volume in a poloidal section.

Fig. 10 Azimuthal variation of the specific turbulence for two different chords : $k = 5\ cm^{-1}$.

a) X = -1.5 cm (crosses for $\theta - \theta_0 > 0$ and open circles for $\theta - \theta_0 < 0$).

b) X = 0 cm (diameter)

The characteristic widths are defined at $1/e^2$.

Fig. 11 Azimuthal variation of the specific turbulence for two symmetrical chords : $k = 7\ cm^{-1}$.

a) $X = 1.5$ cm
b) $X = -1.5$ cm

Fig. 12 Comparison between numerical simulation and experiment : $k = 7\ cm^{-1}$.

Top : azimuthal specific density fluctuation variations.
Bottom : radial profile
Cell parameters $r_0 = 1.7$ cm ; $\Delta\theta_c = 1.2$ rad
$\Delta r_i = 0.3$ cm for $r < r_0$; $\Delta r_e = 2$ cm for $r > r_0$

Fig. 13 Direction of the "sooner and faster" heat flux during the third phase (soft X-ray analysis). θ refers to the azimuthal hot core position.

Fig. 14 Direction of the hot area fast displacement during the second phase (soft X-ray analysis).

Fig. 15 Schematic conclusion. Representation of the turbulence cell ; its azimuthal localization coincides with the "sooner and faster" heat flux.

REFERENCES

[1] VON GOELER, S., STODIEK, W., and SAUTHOOF, N., Phys. Rev. Lett. 33 (1974) 1201.

[2] SHAFRANOV, V.D., Sov. Phys. Tech. Phys. 15 (1970) 175.

[3] ROSENBLUTH, M.N., DAGAZIAN, R.Y. and RUTHERFORD, P.H., Phys. Fluids 16, (1973) 1894.

[4] KADOMTSEV, B.B., Sov. J. Plasma Phys., I (1975) 389.

[5] BUSSAC, M.N., PELLAT, R., EDERY, D., and SOULE, J.L., Phys. Rev. Lett. 35 (1975) 1638.

[6] WADDEL, B.V., ROSENBLUTH, M.N., MONTICELLO, D.A., and WHITE, R.B., Nucl. Fusion 16, 3 (1976).

[7] SAMAIN, A., Plasma Phys., 18 (1976) 551.

[8] COPPI, B., GALVAO, R., PELLAT, R., ROSENBLUTH, M.N., and RUTHERFORD, P., Sov. J. Plasma Phys., 2 (1976) 533.

[9] BUSSAC, M.N., EDERY, D., PELLAT, R., SOULE, J.L., Plasma Phys. Contr. Nucl. Fusion, IAEA, Vol. 1 (1976) 607.

[10] DANILOV, A.F., DNESTROVSKY, Yu.N., KOSTOMAROV, D.P., and POPOV, A.M., Sov. J. Plasma Phys., 2 (1976) 93.

[11] DUBOIS, M.A., and SAMAIN, A., Nucl. Fusion 20 (1980) 1101.

[12] BUSSAC, M.N., PELLAT, R., SOULE, J.L., and TAGGER, M., Phys. Rev. Lett. A. 105 (1984) 51 ; A. 109 (1985) 331.

[13] WESSON, J.A., Plasma Phys. Controlled Fusion 28 (1986) 243.

[14] COPPI, B. et al. Plasma Phys. Contr. Nucl. Fusion, IAEA vol. 3 (1986) 397.

[15] DENTON, R.E., DRAKE, J.F., KLEVA, R.G., and BOYD, D.A., Phys. Rev. Lett. 56 (1986) 2477.

[16] AYDEMIR, A.Y., Phys. Rev. Lett. 59, 6 (1987) 649.

[17] BUSSAC, M.N., PELLAT, R., Phys. Rev. Lett. 59, 23 (1987) 2650.S

[18] WESSON, J., Proceedings of Workshop on Theory of Fusion Plasmas, Varenna, Italy, 24th-28th August 1987, (1987).

[19] CAMPBELL, D.J., GILL, R.D., GOWERS, C.W., WESSON, J., BARTLETT, D.V., BEST, C.H., CODA, S., COSTLEY, A.E., EDWARDS, A.W., KISSEL, S.E., NIESTADT, R.M., PIEKAAR, H.W., PRENTICE, R., ROSS, R.T., TUBBING, B.J.D., Nucl. Fusion Letters 26 (1986) 1085.

[20] CAMPBELL, D.J., DUPERREX, P.A., EDWARDS, A.W., GILL, R.D., GOWERS, C.W., GRANETZ, R.S. et al. Plasma Phys. and Controlled Nuclear Fusion Research, KYOTO, JAPAN (1986) (IAEA, VIENNA, 1987), VOL 1, 433.

[21] EDWARDS, A.W., CAMPBELL, D.J., ENGELHARDT, W.W., FAHRBACH, H.U., GILL, R.D., GRANETZ, R.S., TSUJI, S., TUBBING, B.J.D., WELLER, A., WESSON, J. and ZASCHE, D., Phys. Rev. Lett. 57, 2 (1986) 210.

[22] Equipe TFR and TRUC, A., C.R. ACAD., Sc. PARIS, t.304, Serie II, n°7 (1987).

[23] Equipe TFR and TRUC, A., in 14th European Conf. and Controlled Fusion and Plasma Phys., Madrid, t.3 (1987).

[24] ANDREOLETTI, J., GERVAIS, F., OLIVAIN, J., QUEMENEUR, A., TRUC, A., GRESILLON, D., EUR. CEA-FC 1336 Report (1988). Accepted for Publication in Plasma Phys. and Controlled Fusion.

[25] GERVAIS, F., GRESILLON, D., HENNEQUIN, P., QUEMENEUR, A., TRUC, A., ANDREOLETTI, J., LAVIRON, C., and OLIVAIN, J., 16th European Conference on Controlled Fusion and Plasma Physics. Venezia (1989).

[26] ANDREOLETTI, J., International Workshop on "Turbulence in MHD flows" Cargèse (France) (1988) to be published by Elsevier.

[27] ANDREOLETI, J., 16th European Conference on Controlled Fusion and Plasma Physics. Venezia (1989).

[28] DUBOIS, M.A., PECQUET, A.L., REVERDIN, C., Nucl. Fusion 23, 2 (1983) 147.

[29] TFR Group and TRUC, A., Plasma Phys. and Controlled Fusion 26, 9 (1984) 1045.

[30] TFR Group and TRUC, A., Nucl. Fusion 26, 10 (1986) 1303.

[31] WEISEN, H., HOLLENSTEIN, C.H., and BEHN, R., Plasma Phys. and Controlled Fusion 30, 3 (1988) 293.

[32] BARKLEY, H., GERVAIS, F., OLIVAIN, J., QUEMENEUR, A., TRUC, A., Proceed. Int. Conf. Plasma Physics, Kiev, USSR, April 1987, Vol. 3, 24.

[33] LIEWER, P.C., Nucl. Fusion 25 (1985) 543.

[34] HALLOCK, G.A., MATHEW, J., JENNINGS, W.C., and HICKOK, R.L., Phys. Rev. Lett. 56, 12 (1986) 1248.

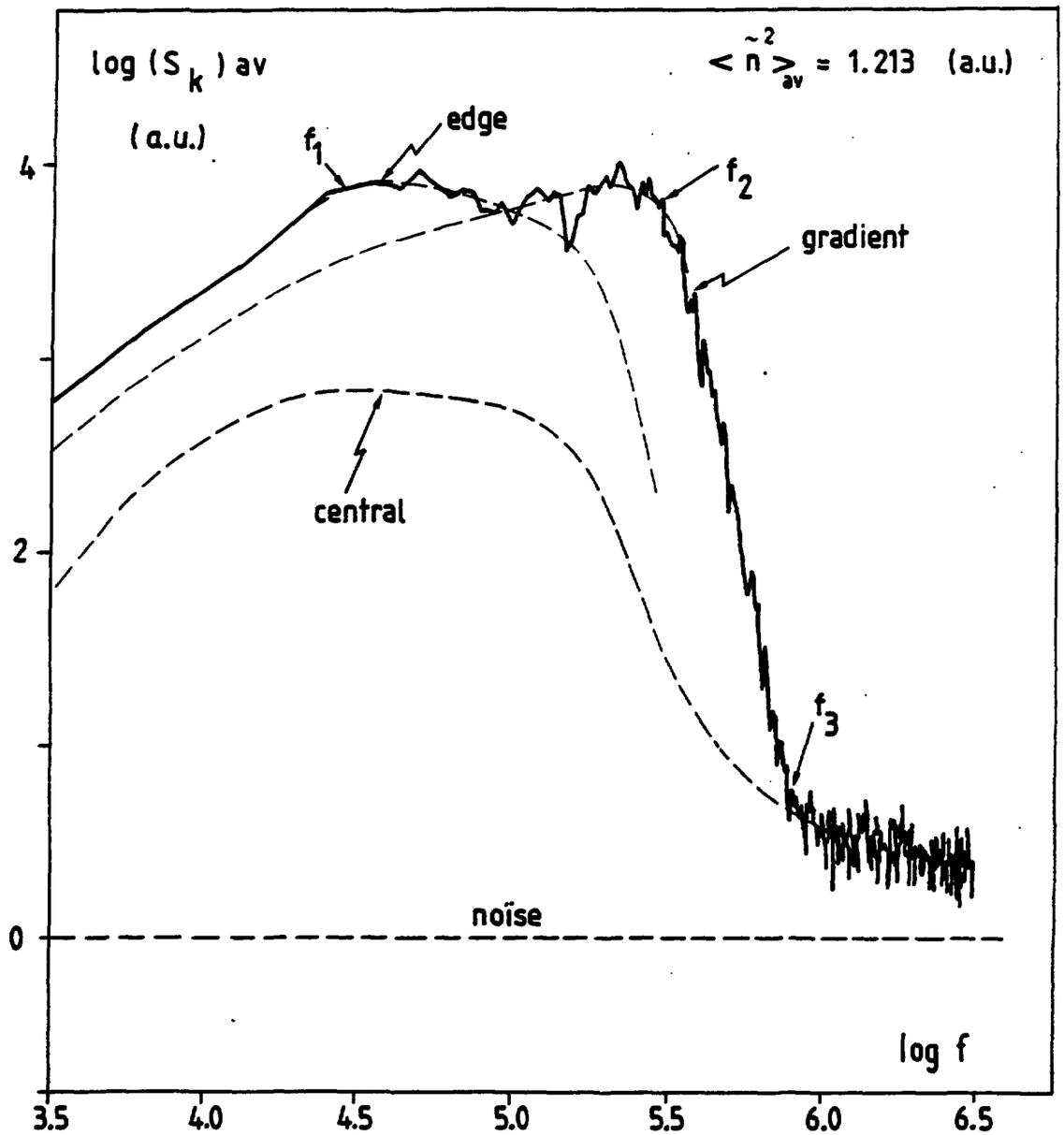
log (S k) av
(a.u.)
< ñ 2 >av = 1.213 (a.u.)
edge
f1
f2
gradient
central
f3
noïse
log f
4
2
0
3.5
4.0
4.5
5.0
5.5
6.0
6.5

FIGURE 1

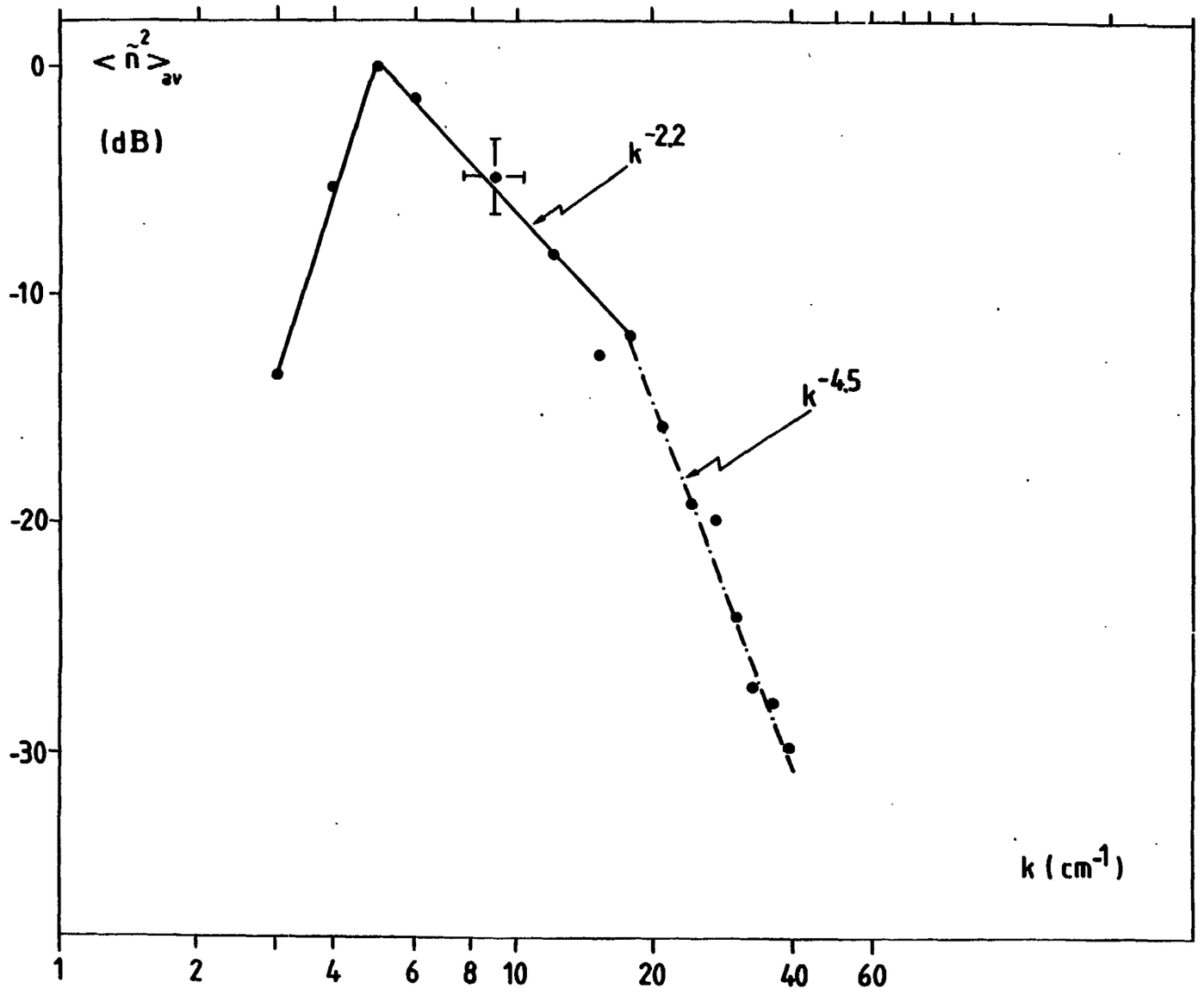
$\langle \tilde{n}^2 \rangle_{av}$
(dB)
0
-10
-20
-30
$k^{-2.2}$
$k^{-4.5}$
k (cm^{-1})
1
2
4
6
8
10
20
40
60

FIGURE 2

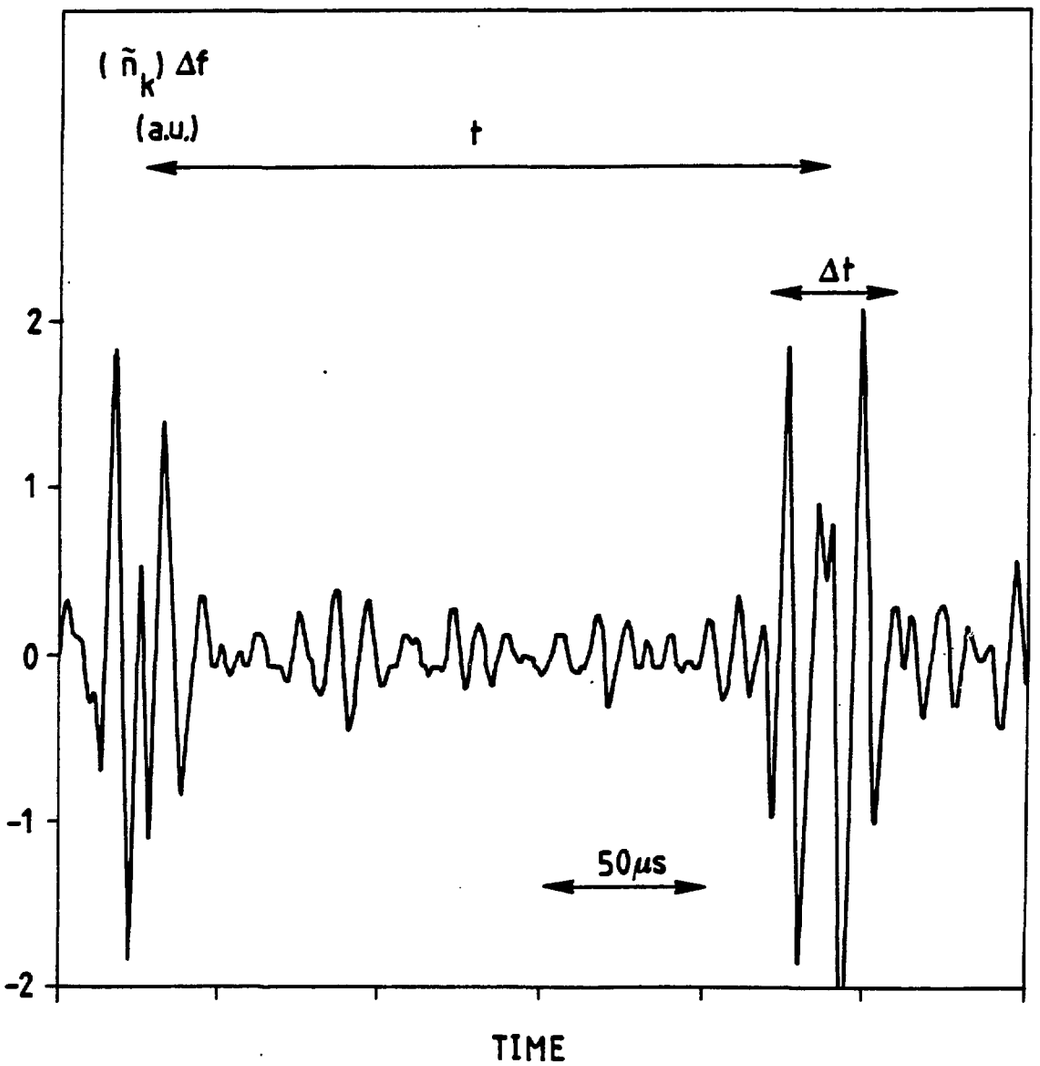

FIGURE 3

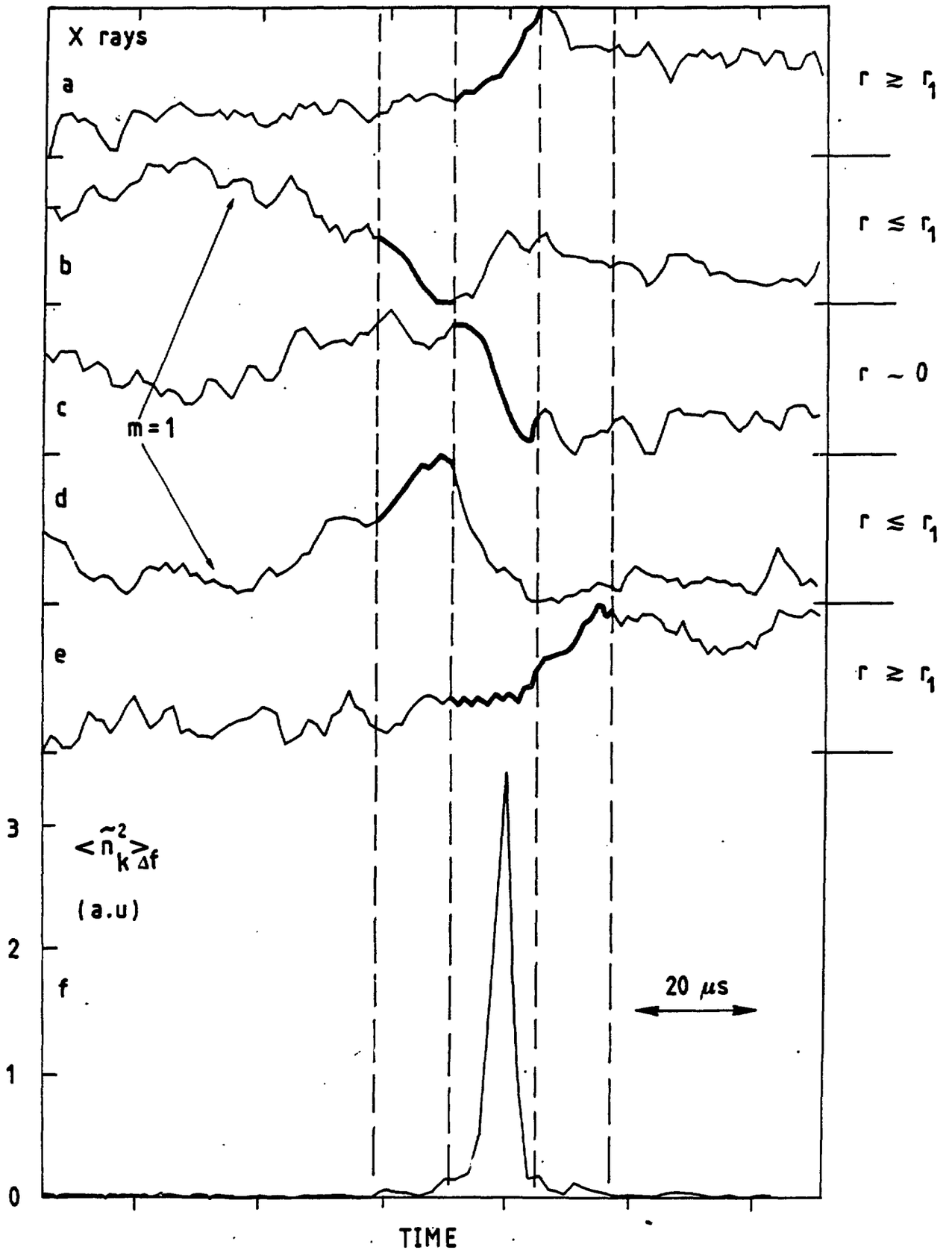

FIGURE 4

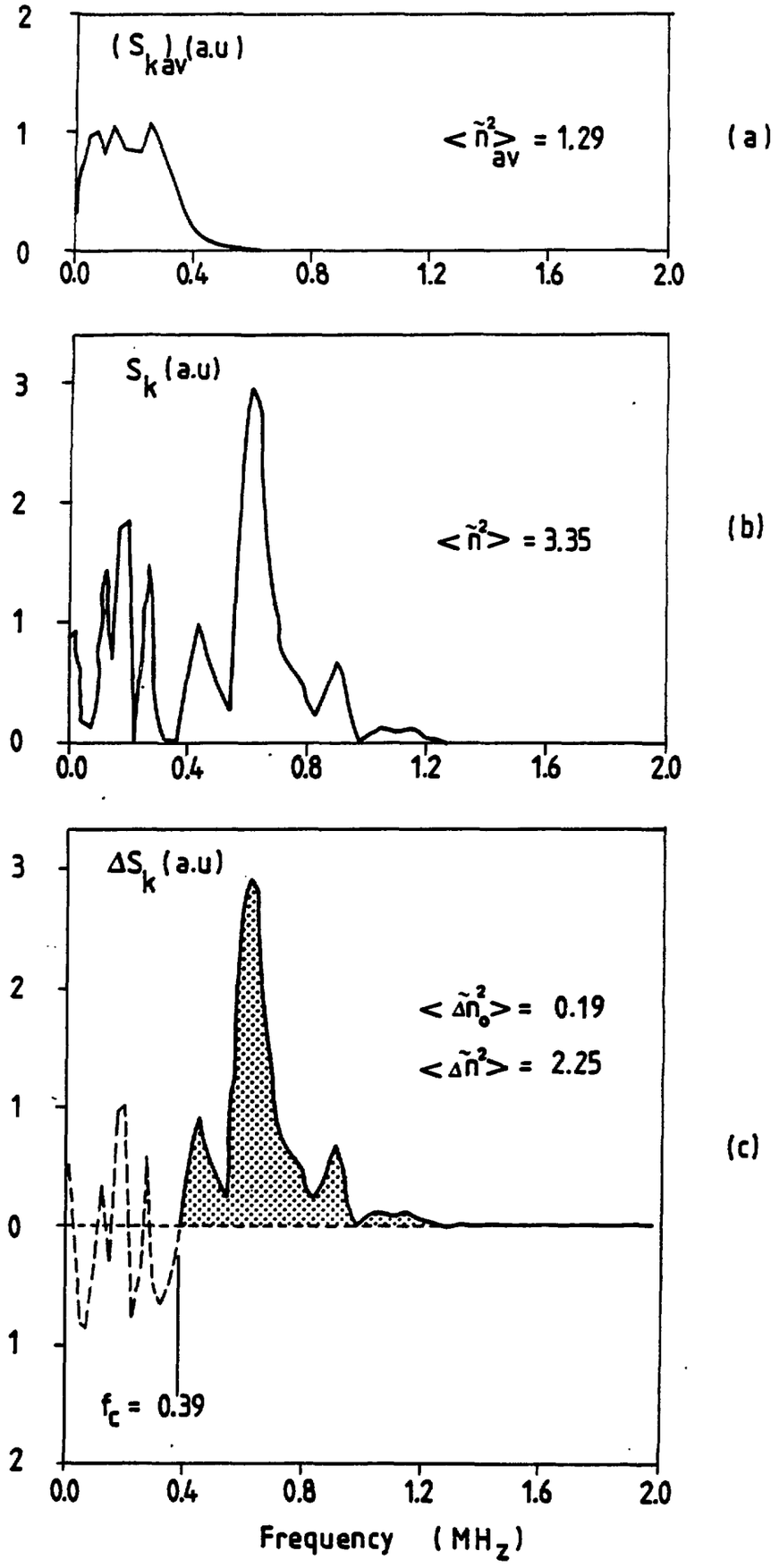
(S_k)_av (a.u)
<ñ²>_av = 1.29
(a)
S_k (a.u)
<ñ²> = 3.35
(b)
ΔS_k (a.u)
<Δñ_o²> = 0.19
<Δñ²> = 2.25
(c)
f_c = 0.39
0.0
0.4
0.8
1.2
1.6
2.0
Frequency (MHz)

FIGURE 5

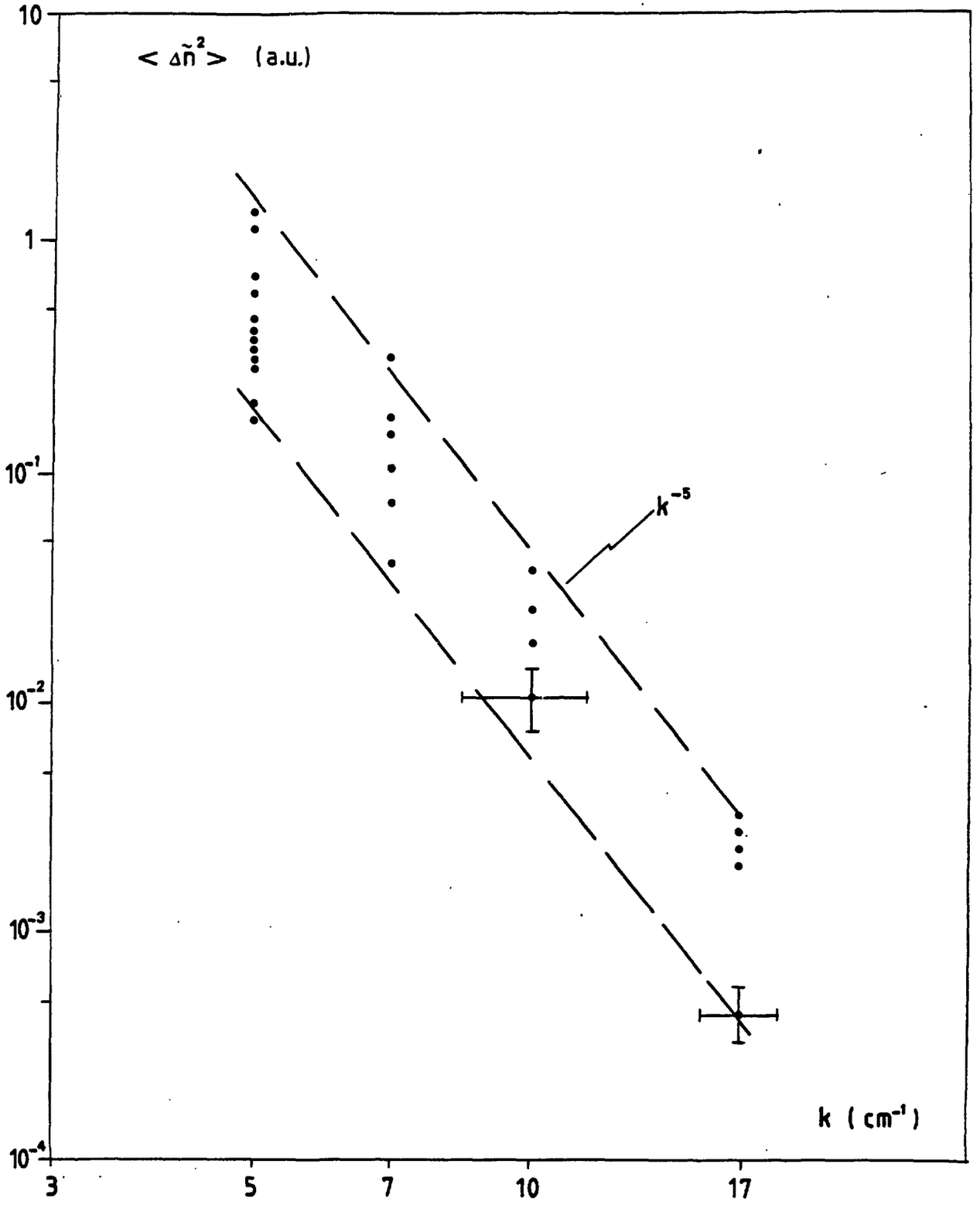

FIGURE 6

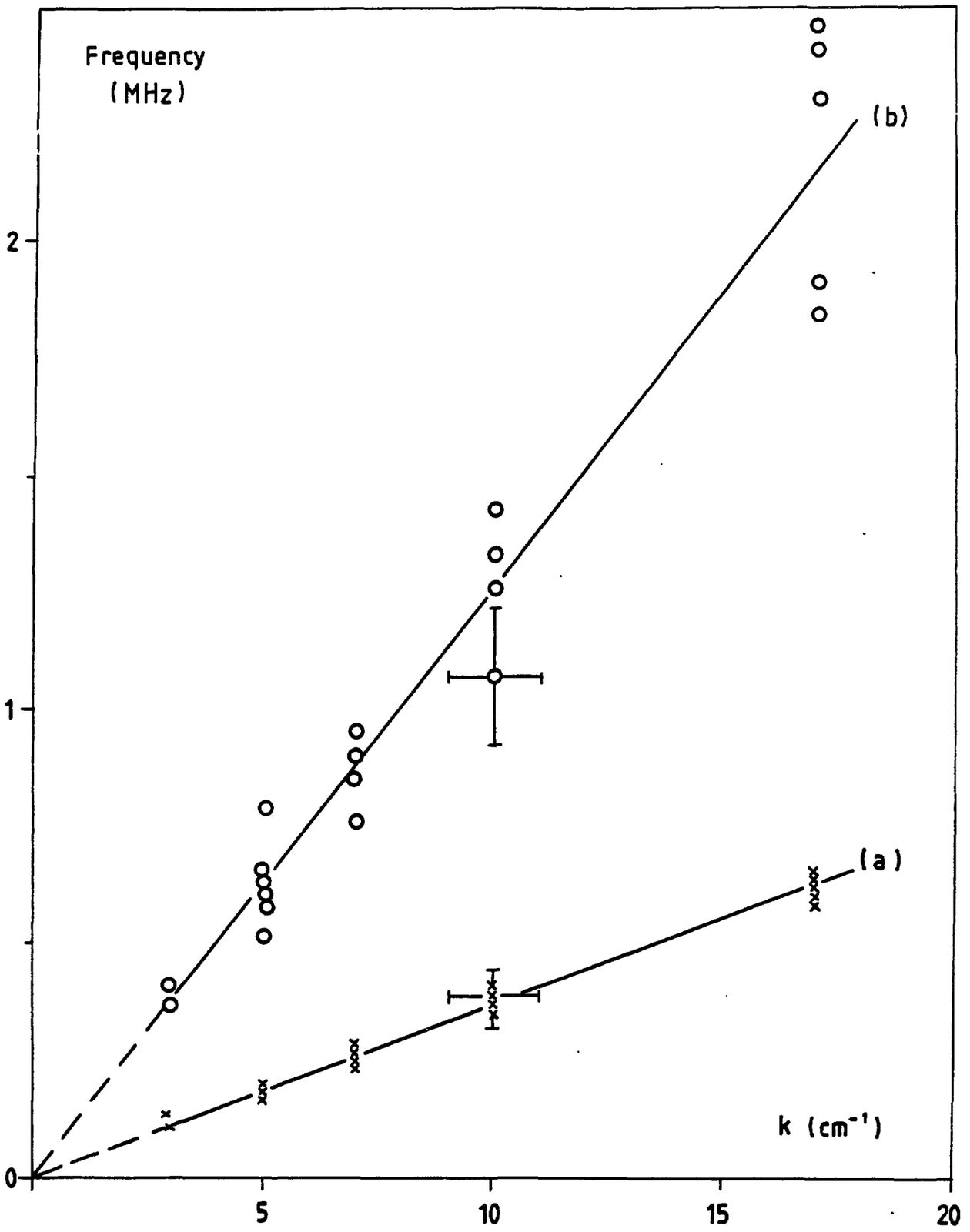

FIGURE 7

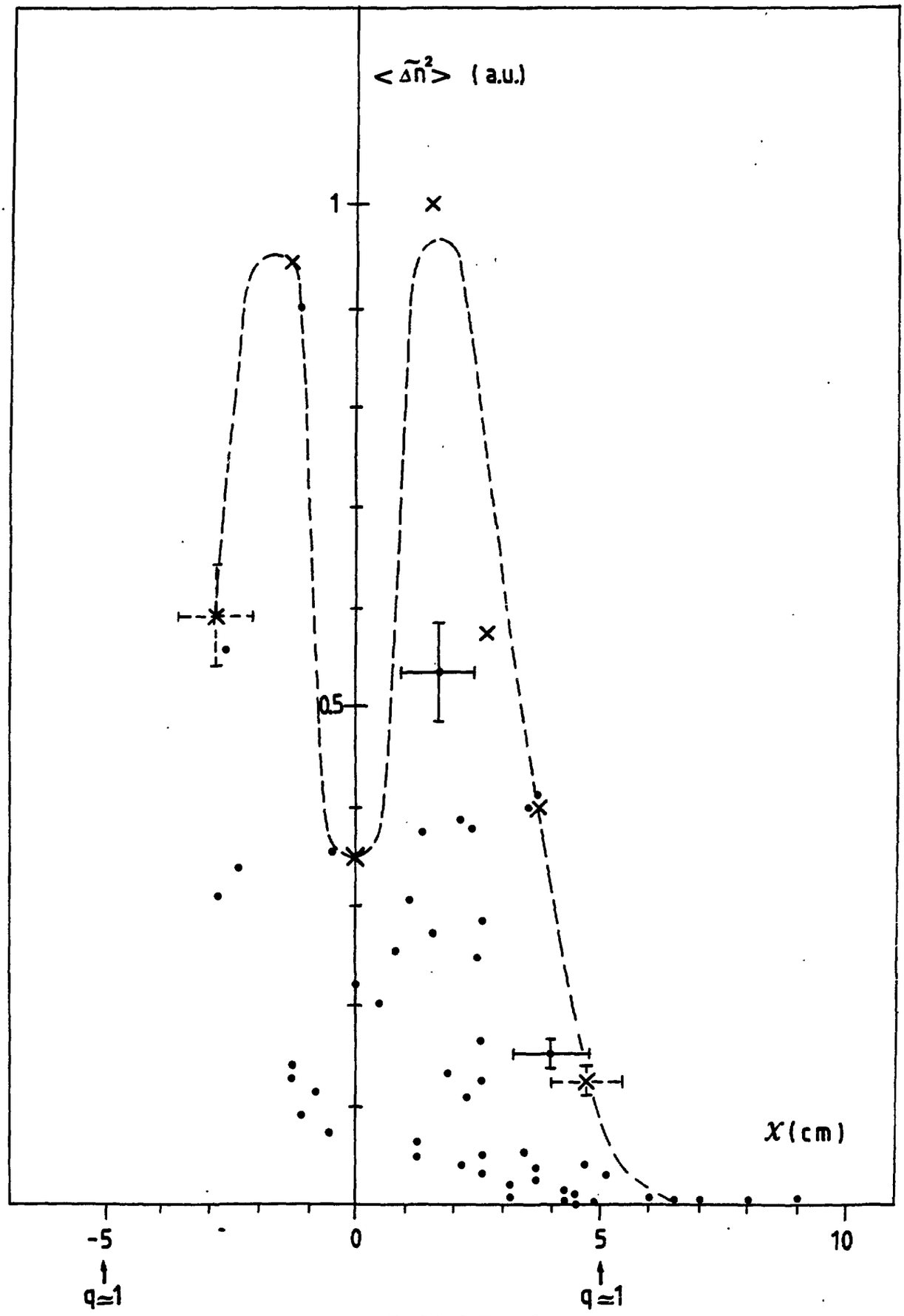

FIGURE 8

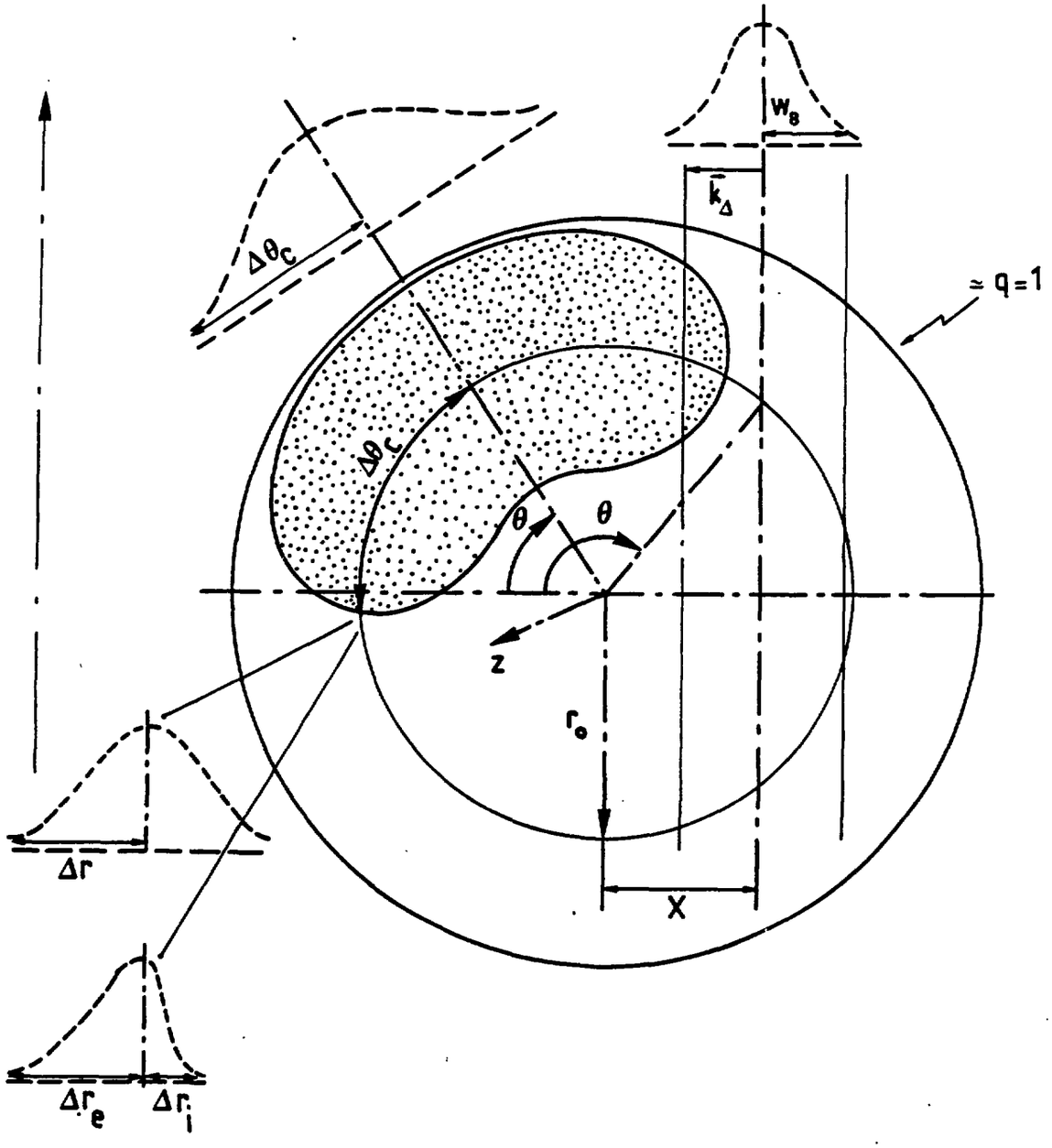
W_s
$\bar{k}_\Delta$
$\Delta\theta_c$
$\simeq q=1$
$\Delta\theta_c$
θ
θ
z
r_o
X
Δr
Δr_e
Δr_i

FIGURE 9

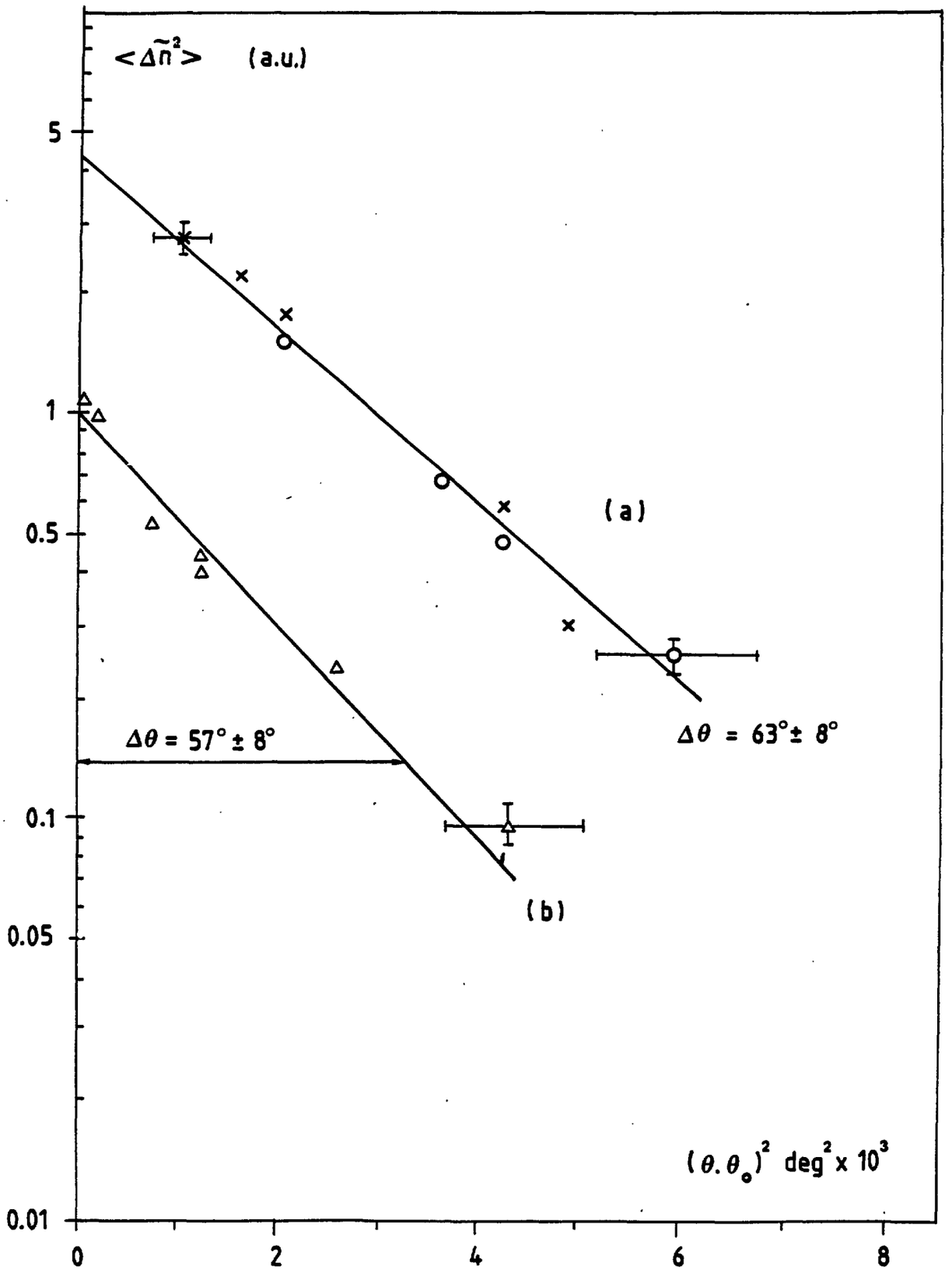
$<\Delta\tilde{n}^2>$ (a.u.)
5
1
0.5
0.1
0.05
0.01
0
2
4
6
8
(a)
(b)
$\Delta\theta = 63° \pm 8°$
$\Delta\theta = 57° \pm 8°$
$(\theta.\theta_o)^2$ deg^2 x 10^3

FIGURE 10

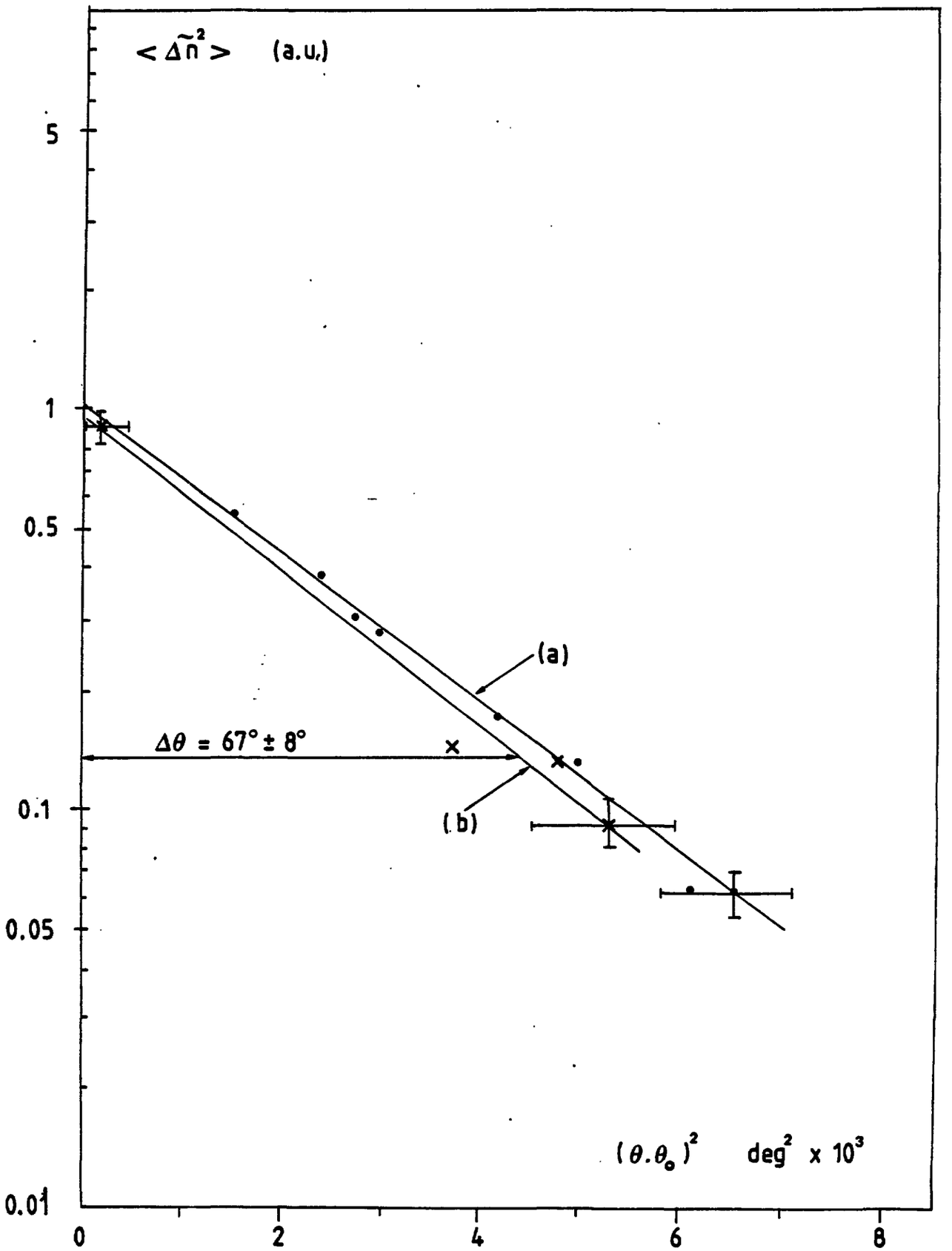
$< \Delta\tilde{n}^2 >$ (a.u.)
5
1
0.5
0.1
0.05
0.01
0
2
4
6
8
(a)
(b)
$\Delta\theta = 67° \pm 8°$
$(\theta.\theta_o)^2$ deg^2 x 10^3

FIGURE 11

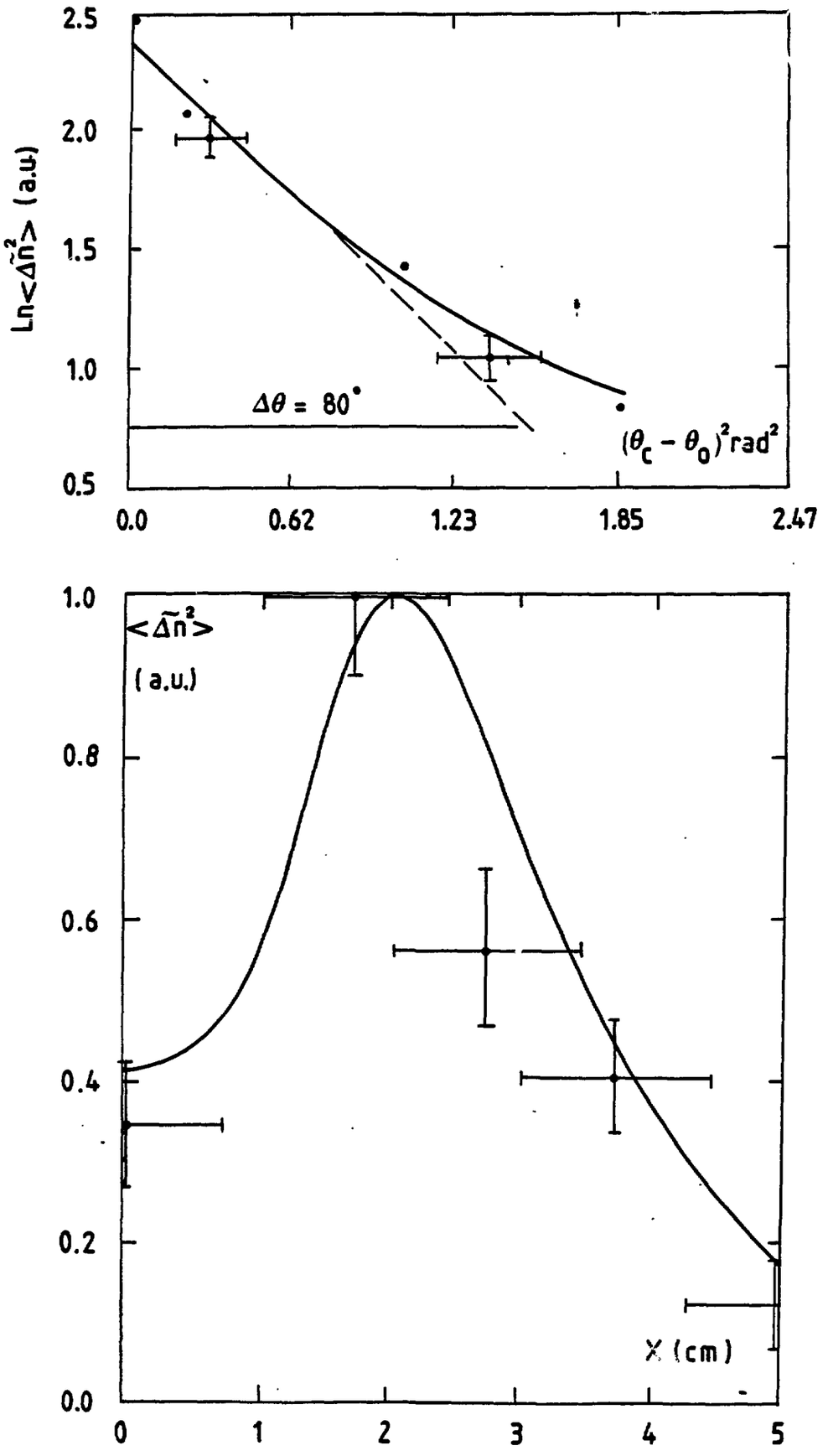
2.5
2.0
1.5
1.0
0.5
Ln<Δñ²> (a.u)
Δθ = 80°
(θc − θ0)²rad²
0.0
0.62
1.23
1.85
2.47
1.0
0.8
0.6
0.4
0.2
0.0
<Δñ²>
(a.u.)
X (cm)
0
1
2
3
4
5

FIGURE 12

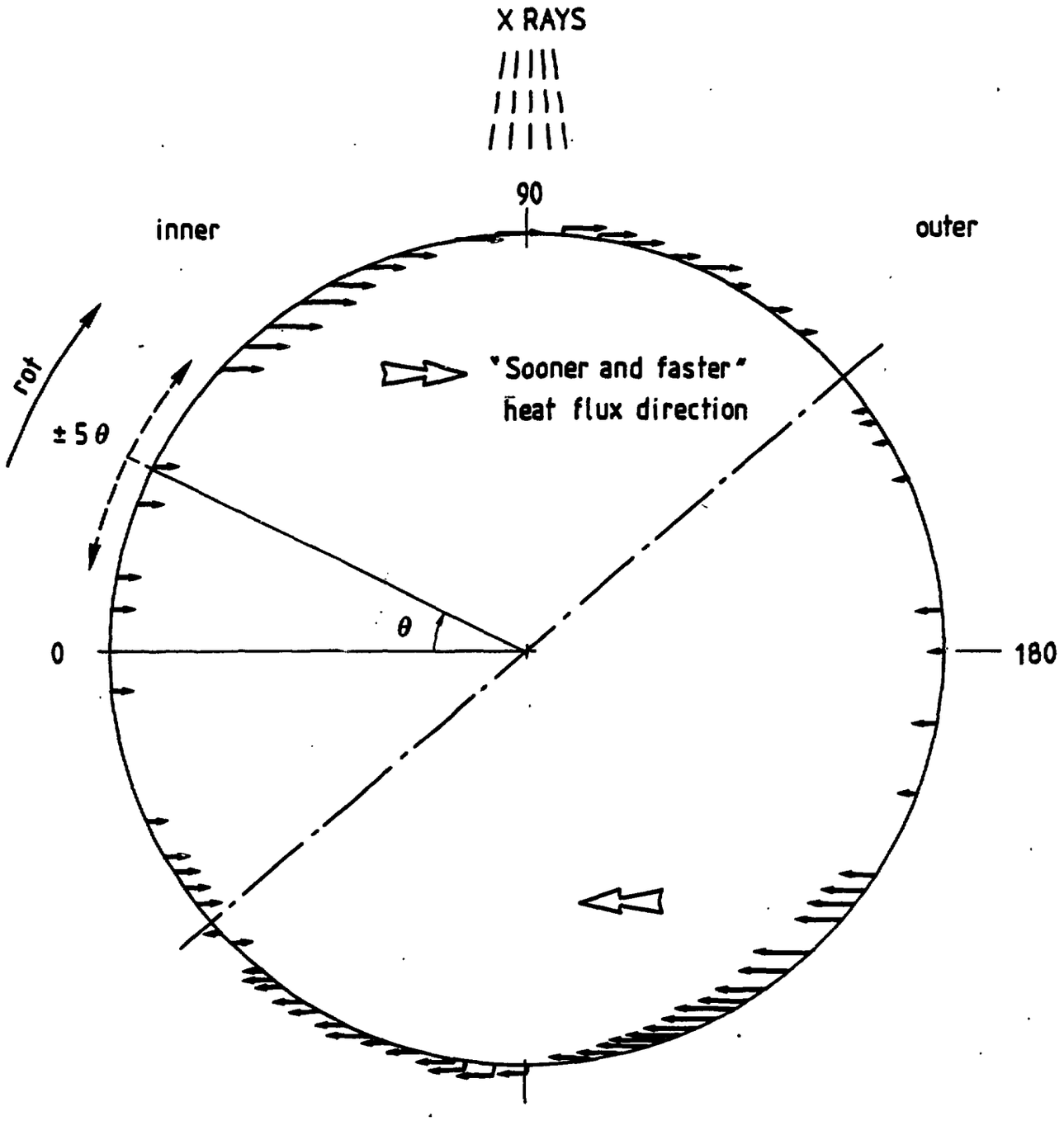
X RAYS
90
inner
outer
rot
±5θ
"Sooner and faster"
heat flux direction
θ
0
180

FIGURE 13

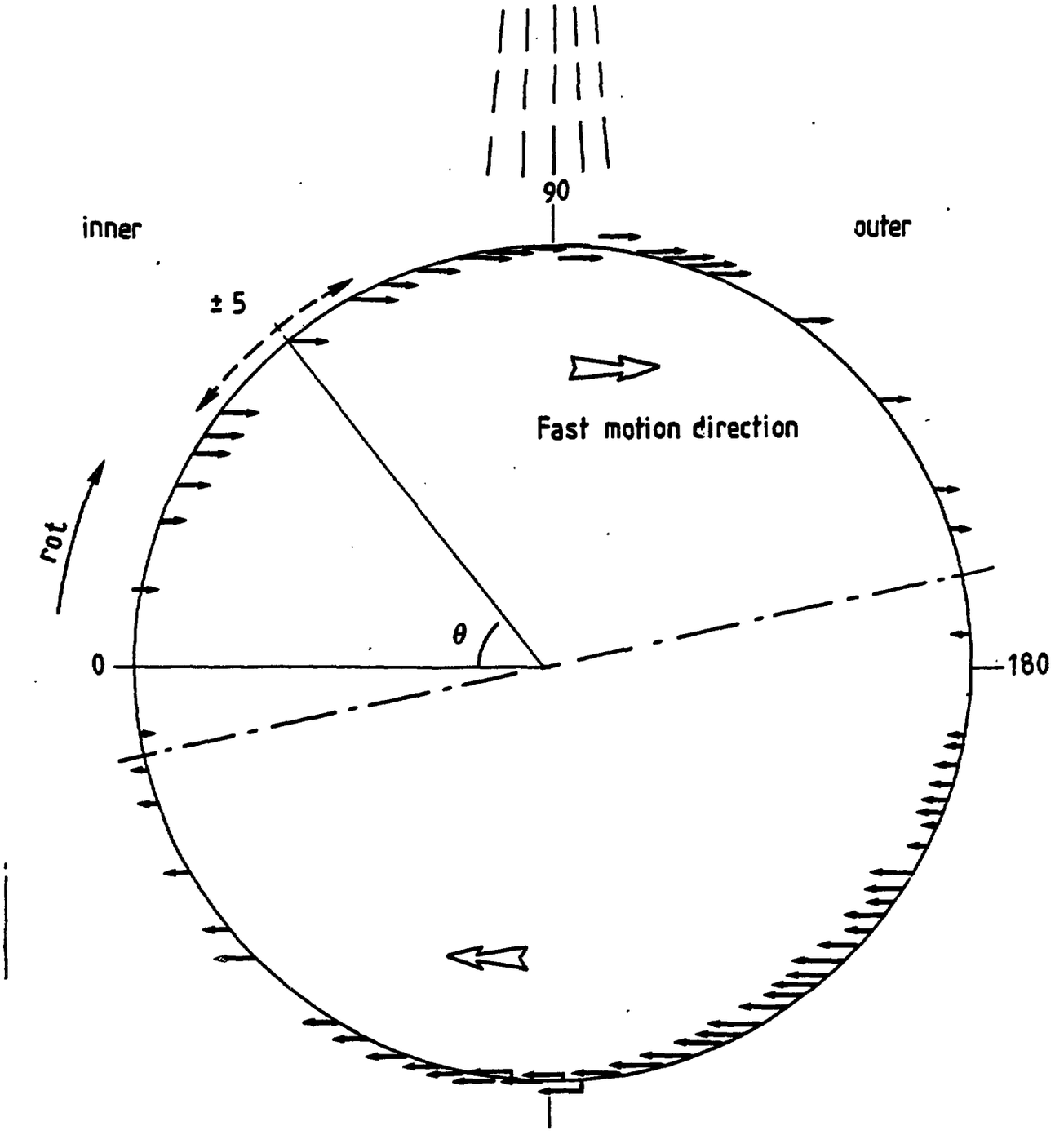

FIGURE 14

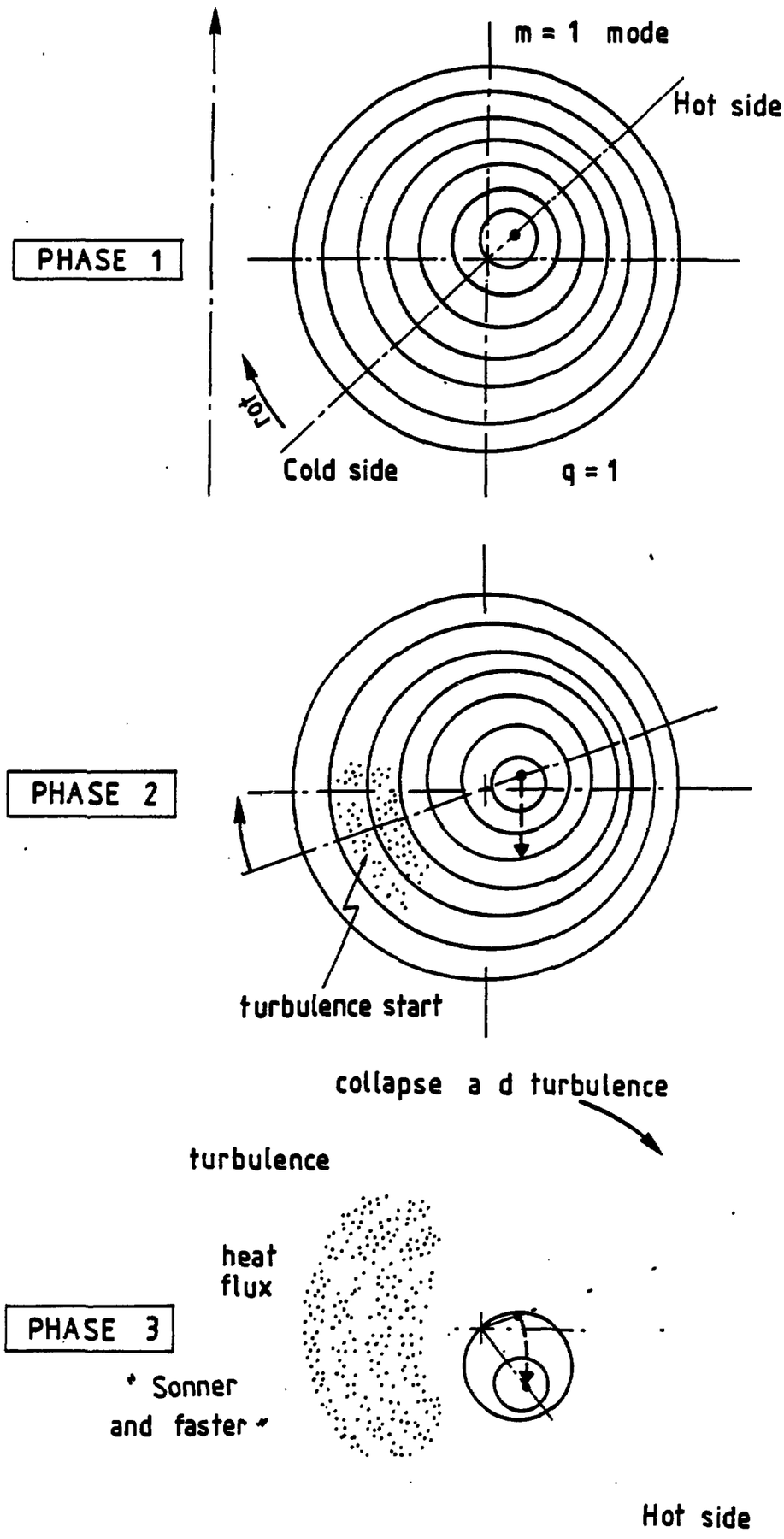
m = 1 mode
Hot side
PHASE 1
Rot
Cold side
q = 1
PHASE 2
turbulence start
collapse a d turbulence
turbulence
heat
flux
PHASE 3
* Sonner
and faster *
Hot side

FIGURE 15